Computer Modeling in Engineering & Sciences CMES, vol.123, no.1, pp.23-47, 2020

A Geometrical Approach to Compute Upper Limb Joint Stiffness

Davide Piovesan[1, *] and Roberto Bortoletto[2]

Abstract: Exoskeletons are designed to control the forces exerted during the physical coupling between the human and the machine. Since the human is an active system, the control of an exoskeleton requires coordinated action between the machine and the load so to obtain a reciprocal adaptation. Humans in the control loop can be modeled as active mechanical loads whose stiffness is continuously changing. The direct measurement of human stiffness is difficult to obtain in real-time, thus posing a significant limitation to the design of wearable robotics controllers. Electromyographic (EMG) recordings can provide an indirect estimation of human muscle force and stiffness, but current methods for the acquisition of the signals limit their use and efficiency. This work proposes a hybrid method for the estimation of upper limb joint stiffness during reaching movements that combines EMG-driven muscle models and constrained optimization. Using these two stages process, we estimated an optimal joints' stiffness bounded in a physiologically sound variability range. This information is crucial when designing exoskeletons user interfaces in which the limb stiffness is an integral part of the control loop. Point-to-point human reaching movements were analyzed to reconstruct the joint stiffness of the upper limb. An accurate 3D model of the arm, encompassing all bones from the hand to the scapula and the majority of the upper limb muscles, was developed to represent the sliding center of rotation of the joints. A well-posed parallel mechanism between the skeleton and the configuration of the tracking markers was implemented. Thus, the muscles' force and joint stiffness were calculated using a generalized pseudo-inversion of the Jacobian transformation between the muscles and Cartesian Space. The maximal and minimal forces exertable by the muscles were set as the boundary condition for the generalized pseudo-inverse by means of a state-of-the-art muscle model.

Keywords: Stiffness, inverse problem, force method, constrained optimization, EMG.

1 Introduction

The control of wearable devices cannot be efficiently designed by assuming that the users' muscle forces are the only means to control body segments dynamics while ignoring the intrinsic mechanical properties of the muscles. The mechanical dynamics of the combined musculoskeletal system play a central role to gain a fuller understanding of the

[1] Biomedical, Industrial and Systems Engineering, Gannon University, 109 University Square, Erie, PA, 16541, USA.

[2] 221e Ltd., Piazza dell'Artigianato, 10, 35031 Abano Terme (PD), Italy.

[*] Corresponding Author: Davide Piovesan. Email: piovesan001@gannon.edu.

Received: 24 November 2019; Accepted: 29 January 2020.

control of movement in its entirety. To control the human body movement, the Central Nervous System (CNS) generates neural commands to activate the muscles. Muscles' force combined with inertia and external forces, results in observable movement. An accepted parameter that has been used to describe the relationship between neural control and limb mechanics is muscle stiffness [Piovesan, Morasso, Giannoni et al. (2013)]. However, the direct measurement of both muscles' force and stiffness is impossible, thus posing an important limitation to the design of wearable robotics controllers.

Methods to obtain muscle force and stiffness rely on numerical models that can be subdivided into two main categories. The first approach is to assume a physiologically sound cost function [Van Bolhuis and Gielen (1999)] that is minimized to resolve the over-constrained problem of having more muscles than Degrees Of Freedom (DOFs) to move [Van Bolhuis and Gielen (1999)]. The second approach is to use the Electromyographic (EMG) signal of muscles as input for a muscle model that can produce a force output [Lloyd and Besier (2003); Shao, Bassett, Manal et al. (2009)]. Methods based purely on cost functions are often not able to represent the co-contraction level of the muscles. Co-contraction is energetically expensive and, if the cost functions to be minimized are based on metabolic energy or similar figures of merit, co-contraction strategies are usually avoided. On the other hand, musculo-skeletal models based on EMG recordings can provide an indirect estimation of human muscle force and estimate the co-contraction levels of muscles' pairs which are directly related to joints' stiffness. However, while EMG-Driven models seem quite appealing, factors such as perspiration and movements of the skin can create EMG artifacts that affect the estimation. Lastly, it is difficult to acquire deep muscles as only superficial muscles are practical to measure for the control of wearable robots. As a consequence, a large number of muscles are ignored.

The complexity of the human arm kinematics and dynamics is evident when the hand is moved to achieve a specific goal in the Cartesian Space while controlling the over-abundant DOFs of wrist, elbow and shoulder girdle at the same time. To clarify this statement, let us analyze a concrete situation such as the simple routine of reaching for a pencil placed on a table. The same final goal (i.e., to grasp the pencil with a well-defined position and orientation of the hand) can be achieved with an infinite number of arm poses since the self-motion manifold of the joint space has a finite dimension [Burdick (1989)]. The number of joints in the upper extremity allows the hand to cross many different paths leading to the same final point. This is because the number of joints in the upper extremity is higher than the DOFs the pencil has in the Cartesian Space. In this context, one of the main difficulties connected to solve the inverse kinematic problem is to discover a general control strategy that allows the selection of the most appropriate trajectories during a given task assuring at the same time the same type of smoothness we can find in natural movements. A common method to analyze the control of the upper limb is to use a reductionist approach where a two-link arm is constrained to move on a plane under the implicit assumption that the duration of the movement is known before its beginning and the shoulder girdle is a simple revolute joint [Piovesan, Pierobon, DiZio et al. (2012, 2013)]. Using such a simple approach some important issues in natural every-day motion might be neglected, including multiple constraint satisfaction, endpoint solution specificity as a function of the task and the generation of complex paths in 3D

space. The model here proposed considers a large number of internal degrees of freedom of the arm which obviates these limitations.

The human arm is not only a kinematically redundant system where, given the position of the hand, an infinite number of self-motions is possible, but is also an over-constrained system where the motion of each link is commanded by multiple actuators (i.e., the muscles) acting together [Kutch and Valero-Cuevas (2012)]. The problem of representing a mechanism as redundant (i.e., over-constrained) has been tackled in the field of structural and applied mechanics [Aghili (2011); Stadlmayr, Witteveen and Steiner (2015); Wojtyra and Frączek (2012)], where it is necessary to estimate if a structure is able to withstand the loads for which it was designed and at the same time limit the maximum deflection given a certain load. Hence, some easy parallelisms can be drawn between system control and structural mechanics resolution methods.

The control of a redundant kinematic chain can be tackled using a stiffness control scheme. This strategy commands the movement of the joints with respect to a reference position and the relative stiffness between the joints themselves to achieve the desired torque and force at the point of contact [Piovesan, Kolesnikov, Lynch et al. (2019)]. In structural mechanics, this is equivalent to solve the indeterminate structural problem using the displacement method [Bauchau and Han (2014); Shin, Lee, In et al. (2010)], where the original system is modified by adding new constraints obtaining a combination of elementary structures whose reaction forces under deformation have been previously studied. The input is displacements in the directions of the added constraints, the output is the reactions force of the imposed deformation which sum must be equal to zero to obtain equilibrium.

Conversely, the over-constrained mechanism can be solved with an explicit compliance control scheme that uses force set-points as commands and accomplishes contact force control directly [Masarati, Morandini and Fumagalli (2014); Piovesan, Kolesnikov, Lynch et al. (2019); Segalman (2007)]. The torque and force at the joint and the compliance of the system determine the position of the joints. This is equivalent to resolve a statically indeterminate problem [Maugh (1946)] in a structure by means of the force method, where constraints are removed from the chosen structural model (e.g., welded junctions are modeled as hinges). The removed constraints are replaced by torques so to obtain a stable and statically determinate structure (virtual forces are imposed resulting in the movement of the structure, which must be zero at equilibrium).

The ultimate goal of this work is to produce the estimation of the joint stiffness by applying the two aforementioned control schemes separately between the joints and the Cartesian Space (redundant/stiffness control) and between the muscle and joint space (over-constrained/compliance control) to solve the redundant/over-constrained control problem of the human arm. The transformation between the three spaces (Cartesian, Joints, Muscles) is done using geometrical transformation establishing the relationship of a generalized pseudo-inverse of the Jacobian matrices via the elastic energy field.

We designed a simulation using SimWise 4D, and VirtualMuscle [Cheng, Brown and Loeb (2000)], using a hybrid approach that can take advantage of the best of both EMG-Driven and optimization-based models. This paper presents the simulation of a closed kinematic chain between a modeled “right human arm and shoulder” on one side, and the kinematic chain of an ad-hoc marker set on the other representing the position of

anatomical landmarks on the "arm and shoulder" in the Cartesian space. Thirty-nine muscles were implemented for which minimum and maximum force were estimated instant-by-instant using the EMG-Driven muscle model while the arm moved along a pre-determined trajectory. This was possible by imposing either a minimum or maximum activation to the muscles while simulating a point-to-point reaching movement enforced onto the simulated arm. The interaction force between the arm and the environment was also estimated, assuming the aforementioned anatomical landmark as point of contact with the environment. Obviously, for an unfettered movement such contact forces ought to be nil. This information allowed for the creation of upper and lower boundaries for both muscle forces and short-range muscle stiffness. Hence, for each instant, the boundaries where used into a constrained optimization aimed at obtaining an estimate of muscles' force that would satisfy the interaction forces between the human and the environment.

2 Methods

2.1 Theoretical background

To summaries the different coordinates and spaces used in this work, we will refer to the following scheme:

$$
\begin{aligned}
&\text{a) Arm Cartesian } \boldsymbol{\Psi} \Rightarrow \begin{cases} \text{position} \\ \text{force} \end{cases} \Rightarrow \begin{cases} \mathbf{y} = \begin{bmatrix} y_1 & y_2 & \cdots & y_r \end{bmatrix}^T \\ \mathbf{F} = \begin{bmatrix} F_1 & F_2 & \cdots & F_r \end{bmatrix}^T \end{cases} \\
&\text{b) Joints } \boldsymbol{\Theta} \Rightarrow \begin{cases} \text{position} \\ \text{force} \end{cases} \Rightarrow \begin{cases} \mathbf{q} = \begin{bmatrix} q_1 & q_2 & \cdots & q_k \end{bmatrix}^T \\ \mathbf{T} = \begin{bmatrix} T_1 & T_2 & \cdots & T_k \end{bmatrix}^T \end{cases} \\
&\text{c) Muscles } \boldsymbol{\Lambda} \Rightarrow \begin{cases} \text{position} \\ \text{force} \end{cases} \Rightarrow \begin{cases} \mathbf{x} = \begin{bmatrix} x_1 & x_2 & \cdots & x_m \end{bmatrix}^T \\ \boldsymbol{\Phi} = \begin{bmatrix} \Phi_1 & \Phi_2 & \cdots & \Phi_m \end{bmatrix}^T \end{cases}
\end{aligned}
\tag{1}
$$

where $\boldsymbol{\Psi}$, $\boldsymbol{\Theta}$, and $\boldsymbol{\Lambda}$ are functors, mapping the generalized positions of the specific vectorial space into a generalized force associated with said topology [Jacobson (2009)].

Let us consider a vector $\mathbf{y} = \begin{bmatrix} y_1 & y_2 & \cdots & y_r \end{bmatrix}^T$ that describes the position and orientation of a specified set of anatomical landmarks on arm in a Cartesian Space. This vector is not strictly representing the operational coordinates often specified in robotics as the position and orientation of the end effector but it rather denotes a set of generalized co-ordinates on the surface of the arm. This formulation is often used when describing Whole-Arm-Manipulations (WAM), as in Salisbury [Salisbury (1987)].

Let $\mathbf{q} = \begin{bmatrix} q_1 & q_2 & \cdots & q_k \end{bmatrix}^T$ be a set of generalized coordinates that fully describes the configuration of the limb joints. Note that, also in this case, q_i is not necessarily a rotation (as in a revolute joint) but it could be a translation (as in a prismatic joint). A mapping between the two spaces can be described as follows:

$\mathbf{y} = \left[W(\mathbf{q}) \right]$.

The map $[W]$, where the dependency from $\mathbf{q}$ has been omitted for convenience, is a Jacobian matrix. Indeed, the relationship between the differential of the co-ordinates in the Cartesian space and those in the joint space can be written as a first approximation as:

$$d\mathbf{y} \cong [W(\mathbf{q})]\, d\mathbf{q}. \tag{2}$$

Due to the redundancy condition, $[W]$ has usually more columns than rows (i.e., $k > r$). Thus, the regular inverse $[W]^{-1}$ does not exist and the inverse kinematics allows an infinite number of solutions.

The DOFs of the human arm are actuated via a sophisticated actuators' network (i.e., the muscles). Thus, the over-constrained relationship between generalized joint torques $\mathbf{T} = [T_1 \quad T_2 \quad \cdots \quad T_k]^T$ and muscle forces $\mathbf{\Phi} = [\Phi_1 \quad \Phi_2 \quad \cdots \quad \Phi_m]^T$, can be written as follows:

$$\mathbf{T} = [B(\mathbf{q})]^T \mathbf{\Phi}. \tag{3}$$

The matrix $[B]$ (where again the dependency from $\mathbf{q}$ has been omitted for convenience) represents the moment arms of the forces with respect to the joints. When trying to invert the matrix $[B]$, the number of muscles is larger than the number of joints (i.e., $m > k$) and thus an infinite number of muscle forces can provide the same torque component T_i. To find a unique solution to this problem several cost functions have been proposed over the years [Bortoletto, Pagello and Piovesan (2014); Hu, Murray and Perreault (2012); Van Bolhuis and Gielen (1999)].

Finally, we can consider the mapping between the coordinates in the Cartesian space (CS) $\mathbf{y}$ and the muscles length $\mathbf{x}$.

$$\mathbf{x} = [M(\mathbf{y})]$$

Again, we can demonstrate that $[M(\mathbf{y})]$ is Jacobian matrix between the displacements $d\mathbf{y}$ and $d\mathbf{x}$ that can be written using the following linear first approximation relationship:

$$d\mathbf{x} \cong [M(\mathbf{y})]\, d\mathbf{y} \tag{4}$$

A congruent stiffness transformation have been proposed [Chen and Kao (2000); Mussa-Ivaldi and Hogan (1991)] as one of the possible generalized inverses providing a bi-univocal mapping between twists (the sets of displacements and rotations) and wrenches (the sets of force and torques) in different spaces.

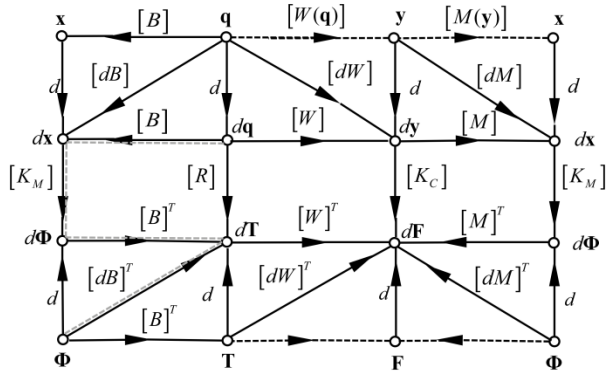

Figure 1: Graph describing the functions that connect the Cartesian Space (CS), the joint space and the muscle space at a certain instant. We assume "*d*" as the function mapping the variable to its differential

The stiffness matrix $[R]$ in Fig. 1 represents the mapping between the differentials of joint angles ($d\mathbf{q}$) and joint torques ($d\mathbf{T}$) so that:

$$d\mathbf{T} = [R]\, d\mathbf{q} \tag{5}$$

Notice that the Joint Stiffness $[R]$ is square and invertible.

A similar relationship can be constructed between the differentials of muscle length ($d\mathbf{x}$) and muscle force ($d\mathbf{\Phi}$) so that:

$$d\mathbf{\Phi} = [K_M]\, d\mathbf{x} \tag{6}$$

$[K_M]$ is a stiffness matrix representing the Short-Range Muscle-Stiffness (SRMS) [Piovesan, Pierobon, DiZio et al. (2013)]. It is worth noting that $[K_M]$ is always invertible, as it is diagonal, full ranked, and all the coefficients on the diagonal are positive. To estimate the muscle stiffness we adopted a model-based approach inspired to previous studies about upper limb [Hu, Murray and Perreault (2011)] and lower limb [Bortoletto, Michieletto, Pagello et al. (2014); Pfeifer, Hardegger, Vallery et al. (2011); Pfeifer, Vallery, Hardegger et al. (2012)]. In particular, a muscle-unit stiffness coefficient can be estimated as a function of the i^{th} muscle force ϕ_i, the Optimal Fiber Length x_{0_i}, and of a dimensionless scaling constant γ [Cui, Perreault, Maas et al. (2008); Piovesan, Pierobon and Mussa Ivaldi (2013)]:

$$K_{M_{ii}} = \frac{\gamma \phi_i}{x_{o_i}} \tag{7}$$

From Fig. 1 the relationship between the differentials of the joint's space generalized coordinates and Cartesian coordinates can be written as:

$$[B]\, d\mathbf{q} = d\mathbf{x} \tag{8}$$

where the matrix of moment arm $[B]$ is also a Jacobian matrix relating twists which elements are the moment arms of the muscles with respect to the joints. Assuming the joint stiffness matrix $[R]$ to be invertible we can combine Eqs. (5)-(7) so that:

$$[B]\left([R]^{-1}\, d\mathbf{T}\right) = [K_M]^{-1}\, d\mathbf{\Phi} \Leftrightarrow \left([K_M][B][R]^{-1}\right) d\mathbf{T} = d\mathbf{\Phi} \tag{9}$$

It is evident that the matrix $\left([K_M][B][R]^{-1}\right)$ is a generalized inverse of $[B]^T$.

Differentiating Eq. (3), we obtain

$$dT_i = \sum_{m=1}^{M} B_{mi} d\Phi_m + \sum_{m=1}^{M} dB_{mi}\Phi_m = d\hat{T}_i + o\left(dT_i\right) \tag{10}$$

using the relationship provided in Eq. (8) to describe the term $o\left(dT_i\right)$ in Eq. (10) and defining the simplified notation $\sum_{k=1}^{K} H_k = \sum_{k} H_k$ yields:

$$\begin{aligned} o\left(dT_i\right) &= \sum_m \left(d\left(\frac{\partial x_m}{\partial q_i}\right)\right)\Phi_m = \sum_m \left(\sum_n \frac{\partial^2 x_m}{\partial q_i \partial q_n} dq_n \right)\Phi_m = \\ &= \sum_n \left(\sum_m \frac{\partial^2 x_m}{\partial q_i \partial q_n}\Phi_m \right) dq_n = \sum_n \Gamma_i dq_n \end{aligned} \tag{11}$$

The substitution of Eq. (11) in Eq. (10) and the use of Eqs. (6) and (8) leads to;

$$d\mathbf{T} = [B]^T\, d\mathbf{\Phi} + [\Gamma] d\mathbf{q} = \left([B]^T [K_M][B] + [\Gamma]\right) d\mathbf{q} \tag{12}$$

Comparing Eq. (12) with Eq. (5) it is immediate to notice the new form of the joint stiffness matrix (i.e., $[R]$). The stiffness $[R]$ is a function of the muscle forces $\mathbf{\Phi}$. Indeed, its components $[\Gamma]$ and $[K_M]$ depend on the muscle force as shown in Eqs. (11) and (7).

The calculation of the muscle force $\mathbf{\Phi}$ is therefore an important factor of this work. We can proceed to estimate $\mathbf{\Phi}$ through the computation of the Cartesian force $\mathbf{F}$ as suggested in Fig. 1 so that;

$$d\mathbf{\Phi} = [M]^{\#T}\, d\mathbf{F} \tag{13}$$

Having found an invertible Jacobian guarantees local inevitability of the function $\mathbf{\Phi}$ [Spivak (2018)]. Furthermore, we can compute the Jacobian of $\mathbf{F}$ by computing the inverse of the Jacobian of $\mathbf{\Phi}$. Indeed, numerous functions that are globally non-invertible can be locally invertible almost throughout their domain (e.g., most even polynomial). Global inevitability can be achieved if an interval can be found where, the Jacobian determinant is everywhere non-zero and $\mathbf{\Phi}$ is proper in the mathematical sense [Hadamard (1906)].

$$\mathbf{\Phi} = \mathbf{\Phi}_0 + \int_{\mathbf{c}(\mathbf{y}_0,\mathbf{y})} \left[M\right]^{\#T} d\mathbf{F} \tag{14}$$

The integral (14) is evaluated by parameterizing the path $\mathbf{c}\left(\mathbf{y_0},\mathbf{y}\right)$ between the initial point $\mathbf{y_0}$ and the position $\mathbf{y}$ and numerically approximating integral. We will see how the calculation of $\mathbf{\Phi}$ is possible by using the multibody software SimWise 4D[2] (Design Simulation Technologies, Inc., Canton, MI, USA)

2.2 Constrained optimization

In this section we will present a hybrid approach to calculate the generalized pseudo-inverse $\left[M\right]^{\#T}$. The Moore-Penrose (MP) pseudo-inverse is in the form:

$$\left[M\right]^{\#T} = \left[\left[M\right]\left[M\right]^T\right]^{-1}\left[M\right]$$

The MP model finds the vector $d\mathbf{\Phi}$, which has the norm $\left|d\mathbf{\Phi}_{null}\right| = 0$ in the null space of matrix $\left[M\right]^T$. This means that any solution given by the MP model corresponds to a solution with minimum norm $\sum_m d\Phi_m^2$ [Klein and Huang (1983)].

The use of the MP approach neglects the following constraints:

1. It does not guarantee a non-negative $\mathbf{\Phi}$ ignoring that the muscles can only pull and never push. While $d\mathbf{\Phi}$ can be negative, indicating that the muscle force is decreasing from a previous point, the force per se cannot be negative.
2. It does not constraint the minimum and maximum amount of force exertable by the muscle
3. It does not take into account additional constraints such as the maximum stiffness obtainable with the maximum force

Calculating $\left[M\right]^{\#T}$ at each instant of time with a linear static optimization allows imposing all of the aforementioned constraints, which we evaluated using a muscle driven model.

2.3 Muscle model

The Virtual Muscles (VM) 3.1.5. software utilizes an algorithm of recruitment of motor units, individually defined as Hill-type muscle models [Cheng, Brown and Loeb (2000)]. The equations that are used to describe a muscle's behavior are fit to data acquired in feline *in vivo* experiment using a Levenberg-Marquardt algorithm [Levenberg (1944); Marquardt (1963)]: a well-known least-squares non-linear curve-fitting technique. For each function, the developers of VM tested numerous possible equations and identified

[2] https://www.design-simulation.com/SimWise4d/

those fitting the data best with minimal complexity and number of coefficients [Brown, Cheng and Loeb (1999); Brown, Kim and Loeb (1998); Brown and Loeb (1999, 2000); Cheng, Brown and Loeb (2000)].

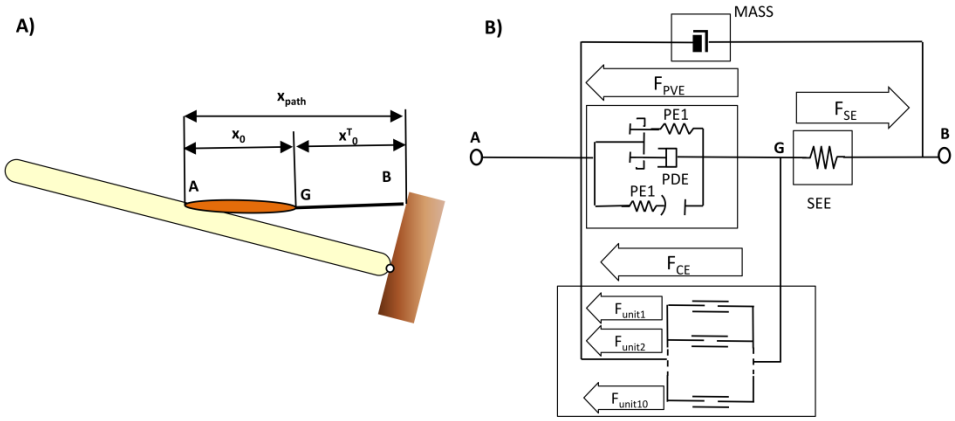

Figure 2: Mechanical scheme for the muscle models as implemented in the software Virtual Muscle (VM). The model's output is the force exerted by the muscle between two bones considered as static and mobile references

Fig. 2(A) Represent a generic muscle actuating a rotational joint. The point A and B represent the insertion of the whole muscle on the bone, point G represent the insertion of the muscle on the tendon. Fig. 2(B) represents a muscle with four main sub-blocks such as, muscle MASS, serial elastic element (SEE) (i.e., the muscle's aponeurosis and tendon), parallel viscoelastic elements (PVE), and contractile elements (CE). PVE can be conceptualized with a spring (PE1) and a damper (PDE) active only when the muscle is elongating, and with just a spring (PE2) when it is shortening. The contractile element is a combination of motor units, which contract with a pre-determined sequence following the Hanneman principle, determined by the size of the motor unit and the activation pattern. Note that the sum of the force of each motor unit will produce the overall force of the contractile element F_{CE}.

$$\begin{cases} \dfrac{(F_{CE}(t)+F_{PVE}(t))-F_{SE}(t)}{Mass_{muscle}} = a_{CE}(t) \\ V_{CE}(t) = \int_{t_o}^{t} a_{CE}(t)dt + V_{init} \\ L_0(t) = \int_{t_o}^{t} V_{CE}(t)dt + L_{init} \end{cases} \tag{15}$$

$$F_{CE} = F_V \cdot (\dot{x},\, x) \cdot F_L(x,t) \cdot A_f(x, f_{eff}, S, Y) \tag{16}$$

VM uses the net force between the contracting F_{CE} element, the parallel viscoelastic element F_{PVE} and the serial elastic F_{SE} element of each muscle to compute the

contracting element velocity V_{CE} and muscle length x_0 necessary for the calculation of the muscular force. Dividing the net force by the muscle mass $Mass_{muscle}$ gives the acceleration of the contracting element. The contractile element velocity and length are calculated by integrating the acceleration a_{CE}, which requires boundary conditions.

Notice in Eq. (16) that the force of the contractile element depends on three components which are function of the force-velocity relationship F_V, the force-length relationship F_L and the activation of the fibers A_f. VM incorporates four first order differential equations to describe the total muscle activation A_f which encompass 1) activation delays, 2) rise and fall time of muscle force, as well as fatigue phenomena such as 3) muscle yield Y (i.e., a fast decrease in muscle apparent stiffness [Brown, Cheng and Loeb (1999)]) and 4) muscle sag S (i.e., a slow decrease in muscle apparent stiffness [Brown and Loeb (2000)]). The equations, dependent on time and motor unit's firing frequency, are implemented for each fiber type and therefore for each motor unit to model physiological behaviors found experimentally. A complete description of the mathematical formulation is provided in Brown et al. [Brown, Kim and Loeb (1998); Brown and Loeb (2000); Cheng, Brown and Loeb (2000); Rack and Westbury (1969); Scott, Brown and Loeb (1996)].

Using a 3D software based on SimWise 4D platform and the kinematic model of the human arm, we reconstructed the trajectories of the arm's bones in the Cartesian Space. Muscles were implemented like actuators in the SimWise environment, and were controlled using a Matlab-Simulink (MathWork) interface. We used VM to simulate the force of the muscles. Assuming that the skeletal model is moved passively along a superimposed reaching trajectory via a set of experimentally recorded whole-arm Cartesian trajectories $\boldsymbol{y}$, the forces that the muscles can apply is directly dependent on the muscles' lengths $\boldsymbol{x}$ and their derivative with respect to time $\dot{\boldsymbol{x}}$, which will uniquely determine F_L and F_V in (16) at the specific instant. On the other hand the total activation A_f depends on the muscles' excitations $\boldsymbol{u}(t)$. We can posit two extreme conditions where all muscles have no excitation $(\boldsymbol{u}(t) = \boldsymbol{0})$, and all muscles have maximum excitation $(\boldsymbol{u}(t) = \boldsymbol{1})$. Therefore, we can calculate a boundary condition for minimum and maximum muscle force and, according to Eq. (7), muscles' stiffness. Notice that even without activation the muscle will produce a passive force given by the interaction between the parallel viscoelastic element and the serial elastic elements as shown in Eq. (15) and Fig. 2B.

2.4 Experimental protocol

The aim of this section is to calculate the force of the muscles in a reaching movement by means of VM, and compute the minimal and maximal stiffness that a subject could exert.

Experimental data where acquired on 10 human subjects in previous experiments of our group. Protocol and instrumental setup are detailed in Piovesan et al. [Piovesan, Pierobon, Dizio et al. (2011); Piovesan, Pierobon, DiZio et al. (2013)]. Each subject was asked to follow with the pointing finger a straight-line trajectory, parallel to the sagittal plane in a movement similar to that of grabbing a pencil that lies on a table.

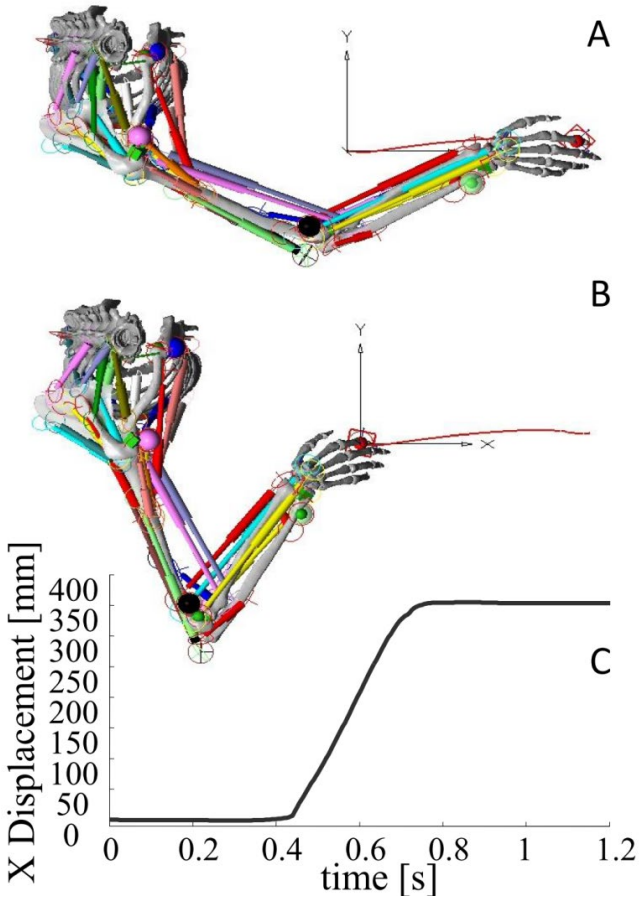

Figure 3: Example of path and trajectory followed by the subjects. The origin of the reference frame is positioned under the index finger in the initial configuration. The x-axis points frontally and the y-axis medially A) Final Configuration B) Initial Configuration. C) time-profile of the displacement along the x axis

Using an Optotrack® system to measure the trajectories described by the subjects' arm, 5 active markers were placed on the latter, located on the index fingertip, styloid process of ulna, lateral epicondyle of humerus, acromion and sternum.

The marker on the sternum was considered as a reference because of the limited mobility of the torso, while the one placed on the scapular part of the acromion was a marker cluster, necessary to record the attitude of the scapular bone. The Cartesian coordinates of the other markers were considered as the description of the position of the arm $\mathbf{y} = \begin{bmatrix} y_1 & y_2 & \cdots & y_r \end{bmatrix}^T$.

A model with joints' sliding center of rotations was used to describe the trajectories of the bones during the set of reaches. Particularly, we constructed a geometrically consistent

closed kinematic chain using two mechanisms in parallel: the skeleton and its articulation on one side and the kinematic chain produced by the markers' movements on the other. In other words, we considered the skeleton as a mechanism which DOFs were driven by the movement of the markers. In our simulation the markers were connected to the skeleton with rigid constrains and driven with the data acquired with the Optotrack system.

Fig. 4 illustrates the coupling of the bone structure (that for brevity we will call here $\sum$) with the kinematic chain created by the markers. For the entire mechanism, the number of DOFs n_{Σ} of Σ are:

$$\begin{aligned} n_{\Sigma} &= 6(m-1) - 5C_1 - 4C_2 - 3C_3 - 2C_4 - C_5 \\ &\vdots = 6(6-1) - 3 \cdot 5 = 15 \end{aligned} \tag{17}$$

where, again, m is the number of links considering also the ground and $C_i \,|\, i = 1, 2, ..., 5$ is the number of joints of a certain class [Shai (2011)]. The class of the joint indicates the number of DOFs that the constrain leaves free. Hence, prismatic and revolute joints are all C_1.

As depicted in Fig. 4 a set of kinematic relationship between the markers and $\sum$ has been introduced by constraining $n_{\Sigma m} = 5 + 3 + 4 + 3 = 15$ DOFs.

Each Cartesian constraint let a coordinate $\mathbf{y} = \begin{bmatrix} y_1 & y_2 & \cdots & y_r \end{bmatrix}^T$ free. We modeled the marker constraint placed onto the scapula, so that the orientation of the bone would be completely predictable. A list of all constrains can be found in in Tab. 1.

The model $\sum$ was used to calculate the force elicited by the muscles, both using a MP pseudo-inverse and a more physiological approach derived by the knowledge of the muscles' properties.

The trajectory (with total duration of 1.2±0.01 s as depicted in Fig. 3) was subdivided into 3000 frames. Using the markers configuration presented in Fig. 4 we could reconstruct a well-posed system between the 15 coordinates of the limb's joints ($\mathbf{q}$) and the 15 Cartesian co-ordinates of the four moving markers and marker cluster ($\mathbf{y}$). For each frame the relationship between the two spaces can be linearized. By applying for each frame a variation of 1 mm or 1 deg to each coordinate y_i and noting the corresponding variation of $d\mathbf{q}$ and $d\mathbf{x}$ it was possible to calculate each components of the Jacobians $[W]$ and $[M]$ in Eqs. (2) and (4).

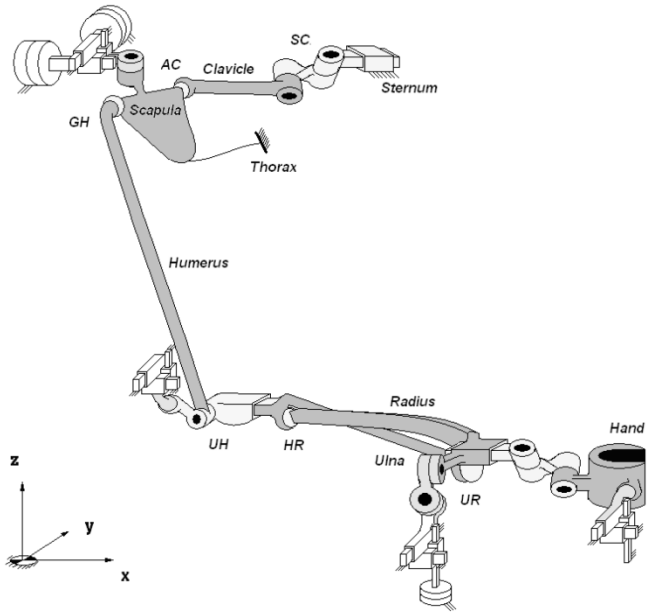

Figure 4: Model of the kinematic chain embedding joints with sliding centers of instantaneous rotations. Light gray joints represent the internal articulation of the mechanism, while the white constrains represent the superimposition of the movement

We superimposed the recorded movement of the real markers onto the model in our simulation. This way, we considered the simulated markers gliding on slides which shapes were those of the recorded trajectories. With our 3D model, we could simulate without ambiguity the movement of the articular joints and the elongations of the muscles.

SimWise 4D requires the inertial properties of each segment and the kinematic constraint between each element as inputs. SimWise 4D calculates the current acceleration of each body in the model given its inertial properties under the generalized displacement $\mathbf{y}$, and uses this acceleration to compute a velocity (and position) one time step later of all segments. Furthermore, SimWise 4D incorporates a scheme to check and correct its prediction. This process is then used again to find a new velocity and position. Because of the particular internal and external constraints' placement illustrated in Fig. 4, as well as the correction algorithm that maintains the constraints congruent it is possible to compute the force vector $\mathbf{F}$ exerted by the skeleton on the slides at each instant of the simulation, depending on the inertial features of the links.

Table 1: Representation of the markers and internal coordinates of model $\sum$. SC=Sternum Clavicular Joint; GH=Gleno Humeral Joint; AC=Acromion Clavicular Joint

q		**y**	
Ry wrist	hand flexion/extension	P1x	displacement fingertip marker dorso-ventral
Rz wrist	hand ad/abduction	P2y	displacement fingertip marker medio-lateral
Rx elbow	prono-supination of the forearm	P3z	displacement fingertip marker vertical
Rz elbow	elbow flexion/extension	P4x	displacement wrist marker dorso-ventral
Ry SC	first rotation of SC	P5y	displacement wrist marker medio-lateral
Rx SC	second rotation of SC	P6z	displacement wrist marker vertical
Rx GH	gleno-humeral ab-adduction	P7x	displacement elbow marker dorso-ventral
Ry GH	gleno-humeral flex-extension	P8y	displacement elbow marker medio-lateral
Rz GH	gleno-humeral int-ext rotation	P9z	displacement elbow wrist marker vertical
Rx AC	Acromio-clavicular ab-adduction	P10x	displacement shoulder marker dorso-ventral
Ry AC	Acromio-clavicular flex-extension	P11y	displacement shoulder marker medio-lateral
Rz AC	Acromio-clavicular int-ext rotation	P12z	displacement shoulder wrist marker vertical
Pz wrist	axial movement of the wrist	R13x	rotation of the wrist marker around x
Px elbow	axial movement of the elbow	R14x	rotation of the shoulder marker around x
Pz AC	axial movement of the clavicle	R15y	second rotation of the shoulder marker around y

By knowing the forces $\mathbf{F}$ we can calculate the muscle force $\mathbf{\Phi}$, using the constrained pseudo-inverse of $\left[M\right]^T$ and integration along the pre-imposed trajectory as previously described in the method section. The constraint to the optimization were the maximum and minimum $\mathbf{\Phi}$ calculated using VM and the maximum muscle stiffness $\left[K_M\right]$ obtained using the length of the muscle and the maximum force at the specific instant as input for Eq. (7). Thus, we computed the matrix $\left[B\right]^{\#}$ after we calculated $\left[\Gamma\right]$ and $\left[K_M\right]$ using Eqs. (11) and (6).

3 Results

During the superimposition of the movement for the whole recorded trajectory we were able to monitor all the muscles' length changes, so that we could use these data as an input for the VM models mentioned above. The introduction of maximal and minimal activation of the muscle throughout the trajectory would bring the maximum and minimum force that all the muscles would exert in that particular instant and with that particular velocity.

Fig. 5 shows the force Root Mean Square (RMS) of each muscle of our model, along the superimposed trajectory. It can be seen that the force calculated using the pseudo inverse $\left[M\right]^{\#T}$ always lies between the minimum and maximum force calculated with the activation driven model.

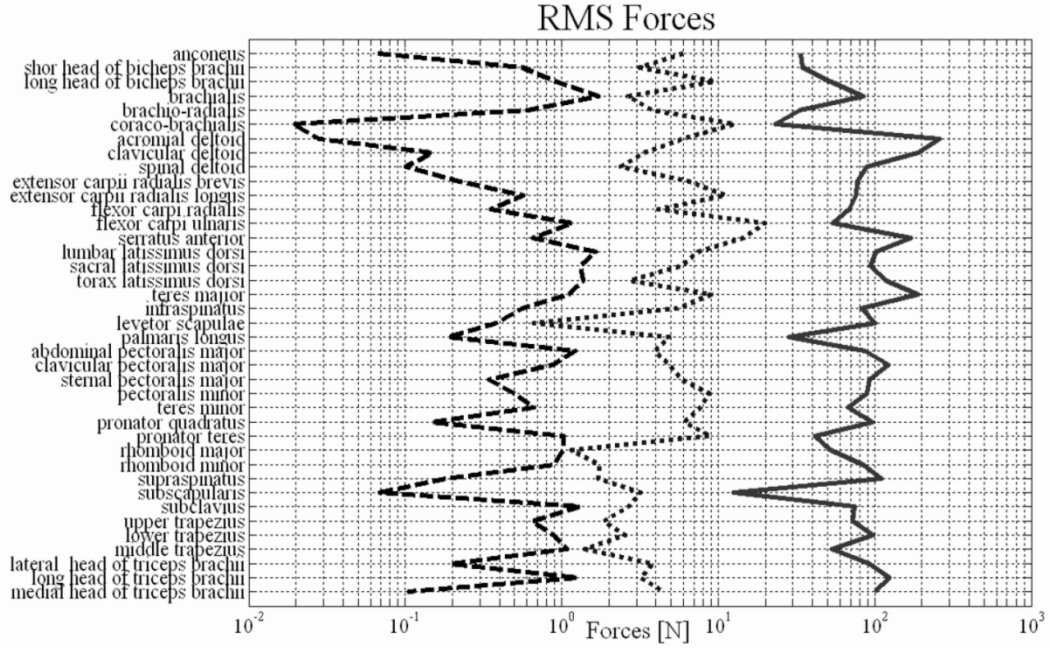

Figure 5: RMS force of each muscle along the movement. Solid) maximum activation, Dashed) minimum activation, Dotted) inverse dynamics

Introducing the forces in Eqs. (7) and (11) on a frame by frame basis, we could calculate the joint stiffness matrix R from Eq. (12) throughout the trajectory.

The value of the elbow rotational stiffness $R_{Z_{elbow}}$calculated with the inverse dynamic method varies between 82.62 to 9.61 [Nm/rad] whereas the value calculated with maximal activation is between 251 and 43 [Nm/rad]. The estimates of $R_{Z_{elbow}}$ as function of time are always within the experimental error provided by Piovesan et al. [Piovesan, Pierobon, DiZio et al. (2013)]. It is also evident the tendency of the stiffness to decrease during movement, again in line with the experimental findings in Piovesan et al. [Piovesan, Pierobon, DiZio et al. (2013)].

For the shoulder rotational stiffness $R_{Z_{GH}}$ the inverse dynamic method yields values between 5.45 to 16.02 Nm/rad. The value of $R_{Z_{GH}}$ calculated with maximal activation is between 11.2 and 19.97 Nm/rad. Again, both values are within the experimental error provided by Piovesan et al. [Piovesan, Pierobon, DiZio et al. (2013)] with a similar tendency of the stiffness time-profile to increase monotonically throughout the movement.

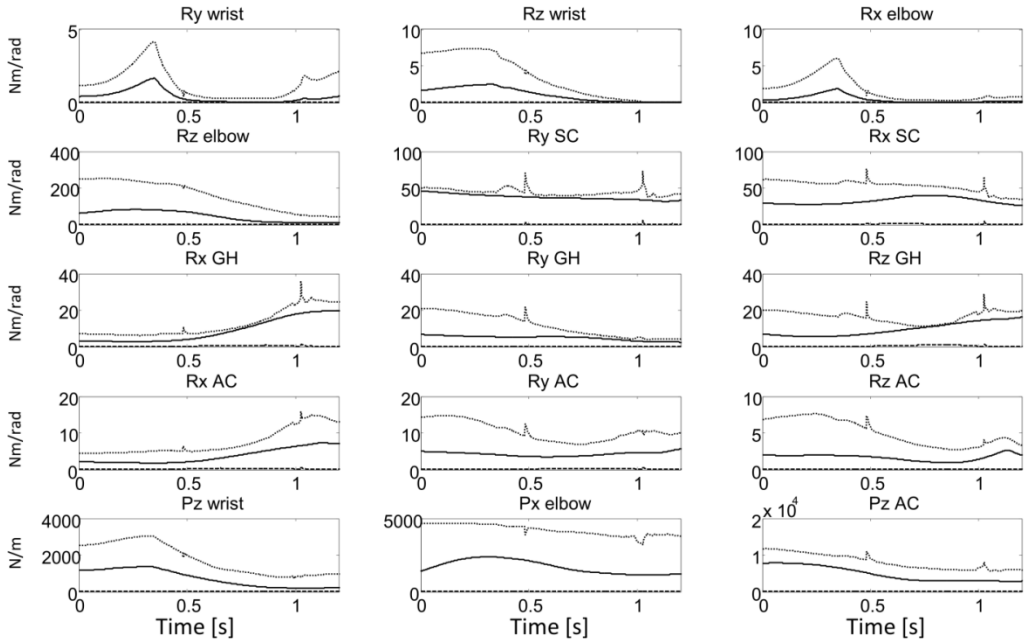

Figure 6: Time profiles of stiffness for the generalized joint $\mathbf{q}$ as reported in Tab. 1. Minimum (dashed line) and maximum (dotted line) joint stiffness are obtained using the value of force at minimum and maximum activation via VM. Optimized stiffness (solid line) was obtained through the inverse Jacobian $[M]^{\#T}$

We also found that the MP estimates of both wrist flexion/extension $R_{Y_{wrist}}$ and ad/abduction $R_{Z_{wrist}}$ stiffness were compatible with the experimental measurement reported in Formica et al. [Formica, Charles, Zollo et al. (2012)] with a maximum of 1.65 and 2.49 Nm/rad, respectively. This maximum value occurs at 0.33 s right before the beginning of the finger movement. Radial prono-supination $R_{X_{elbow}}$ was also maximal after the movement initiation phase with a peak of 1.95 Nm/rad also compatible with experimental measurements [Drake and Charles (2014)].

The axial movement of elbow and wrist along the prismatic joints depicted in Fig. 4 mostly elicit a stretching of the muscles along their line of action. The maximum values of the stiffness are $P_{X_{elbow}}$=2386 N/m and $P_{Z_{wrist}}$=1372 N/m. The contractions of the muscles keep the metacarpal joints connected to the forearm and the forearm connected to the humerus, respectively. The stiffness is of the same order of magnitude of the muscles stiffness $K_{M_{ii}}$ around the prismatic joints acting in parallel.

4 Discussion and conclusion

This study implemented a 3D model of the upper limb. The force of 39 muscles was calculated considering many DOFs often neglected during arm reaching movements. With this work, we found a configuration for the joint structure, combined with a markers' placement on the body that allowed us to calculate the inverse dynamics of the human

arm, with no redundancies between whole-arm and joint space. The relationship between the external marker movements and the modeled mechanism of the upper limb can be treated as a parallel robot or a wearable device interacting with the arm. This allows us finding the reaction forces that virtually should be applied between an exoskeleton and the arm if the markers would be the point of contact between the arm and the exoskeleton moving along a pre-determined trajectory. This method is equivalent to the applying the force method on a structure. The virtual forces applied to the arm combined with the recorded kinematics can provide the virtual work necessary to move the arm. For the principle of virtual work the elastic energy provided by the muscle must be the same. We calculated the force that the muscles could apply between joints, as well as their stiffness using an optimization based on phenomenological aspects.

A physiological approach was used to calculate the maximum and minimum muscle force and stiffness along the trajectory, considering the relation between muscle force and activation being monotone.

We investigated the force that the implemented muscles could apply to the mechanism with no activation and maximal activation, developing a range of possible values of the muscle-stiffness components. We want to highlight that the results achievable using our optimized inverse method are comparable to those obtained experimentally for different upper-limb joints. Moreover, the ability of the proposed technique to provide a subject-specific and task-specific physiologically consistent range of variability of joint stiffness could be effectively used to modulate the metabolic cost in individuals wearing orthotic devices and to better understand abnormal stiffness strategies in patients with neurological and orthopedic conditions in order to setup personalized rehabilitation procedures that restore physiological properties.

It is worth noting that the present analysis have some limitations. First, it requires the use of Jacobian matrices that are computationally expensive to calculate. Second, at the time of this study, the whole analysis loop is implemented in an offline manner allowing for a preliminary setup of a wearable robot control loop. Future work will focus on the improvement of the highlighted limitations through the introduction of a multidimensional spline based approach in order to substitute the use of Jacobian matrices and the integration of the proposed technique in an online loop to effectively use the hybrid inverse dynamics estimation and corresponding joint stiffness information within a control loop of an assistive wearable device.

Funding Statement: The authors received no specific funding for this study.

Conflicts of Interest: The authors declare that they have no conflicts of interest to report regarding the present study.

References

Aghili, F. (2011): Control of redundant mechanical systems under equality and inequality constraints on both input and constraint forces. *Journal of Computational and Nonlinear Dynamics*, vol. 6, no. 3, pp. 031013-031013.

Bauchau, O. A.; Han, S. (2014): Three-dimensional beam theory for flexible multibody dynamics. *Journal of Computational and Nonlinear Dynamics*, vol. 9, no. 4, pp. 041011-041011.

Bortoletto, R.; Michieletto, S.; Pagello, E.; Piovesan, D. (2014): Human muscle-tendon stiffness estimation during normal gait cycle based on gaussian mixture model. *Proceedings of the 13th International Conference on Intelligent Autonomous Systems (IAS-13)*.

Bortoletto, R.; Pagello, E.; Piovesan, D. (2014): Lower limb stiffness estimation during running: the effect of using kinematic constraints in muscle force optimization algorithms. In D. Brugali; J. Broenink; T. Kroeger; B. Mac Donald (Eds.) *Simulation, Modeling, and Programming for Autonomous Robots*, pp. 364-375, Springer International Publishing: New York, USA.

Brown, I. E.; Cheng, E. J.; Loeb, G. E. (1999): Measured and modeled properties of mammalian skeletal muscle. Ii. The effects of stimulus frequency on force-length and force-velocity relationships. *Journal of Muscle Research and Cell Motility*, vol. 20, no. 7, pp. 627-643.

Brown, I. E.; Kim, D. H.; Loeb, G. E. (1998): The effect of sarcomere length on triad location in intact feline caudofeomoralis muscle fibres. *Journal of Muscle Research and Cell Motility*, vol. 19, no. 5, pp. 473-477.

Brown, I. E.; Loeb, G. E. (1999): Measured and modeled properties of mammalian skeletal muscle. I. The effects of post-activation potentiation on the time course and velocity dependencies of force production. *Journal of Muscle Research and Cell Motility*, vol. 20, no. 5-6, pp. 443-456.

Brown, I. E.; Loeb, G. E. (2000): Measured and modeled properties of mammalian skeletal muscle. Iv. Dynamics of activation and deactivation. *Journal of Muscle Research and Cell Motility*, vol. 21, no. 7, pp. 33-47.

Burdick, J. W. (1989): On the inverse kinematics of redundant manipulators: characterization of the self-motion manifolds. In Advanced Robotics: 1989, pp. 25-34, Springer: New York, USA.

Chen, S. F.; Kao, I. (2000): Conservative congruence transformation for joint and cartesian stiffness matrices of robotic hands and fingers. *International Journal of Robotics Research*, vol. 19, no. 9, pp. 835-847.

Cheng, E. J.; Brown, I. E.; Loeb, G. E. (2000): Virtual muscle: a computational approach to understanding the effects of muscle properties on motor control. *Journal of Neuroscience Methods*, vol. 101, no. 2, pp. 117-130.

Cui, L.; Perreault, E. J.; Maas, H.; Sandercock, T. G. (2008): Modeling short-range stiffness of feline lower hindlimb muscles. *Journal of Biomechanics*, vol. 41, no. 9, pp. 1945-1952.

Drake, W.; Charles, S. (2014): Passive stiffness of coupled wrist and forearm rotations. *Annals of Biomedical Engineering*, vol. 42, no. 9, pp. 1853-1866.

Formica, D.; Charles, S. K.; Zollo, L.; Guglielmelli, E.; Hogan, N. et al. (2012): The passive stiffness of the wrist and forearm. *Journal of Neurophysiology*, vol. 108, no. 4, pp. 1158-1166.

Hadamard, J. (1906): Sur les transformations ponctuelles. *Bulletin de la Société Mathématique de France*, vol. 34, pp. 71-84.

Hu, X.; Murray, W. M.; Perreault, E. J. (2011): Muscle short-range stiffness can be used to estimate the endpoint stiffness of the human arm. *Journal of Neurophysiology*, vol. 105, no. 4, pp. 1633-1641.

Hu, X.; Murray, W. M.; Perreault, E. J. (2012): Biomechanical constraints on the feedforward regulation of endpoint stiffness. *Journal of Neurophysiology*, vol. 108, no. 8, pp. 2083-2091.

Jacobson, N. (2009): *Basic Algebra*. Dover Publications. New York, NY, USA.

Klein, C.; Huang, C. H. (1983): Review of pseudoinverse control for use with kinematically redundant manipulators. *IEEE Transactions on Systems, Man and Cybernetics*, no. 2, pp. 245-250.

Kutch, J. J.; Valero-Cuevas, F. J. (2012): Challenges and new approaches to proving the existence of muscle synergies of neural origin. *PLoS Computational Biology*, vol. 8, no. 5, pp. e1002434.

Levenberg, K. (1944): A method for the solution of certain problems in least squares *Quarterly of Applied Mathematics*, vol. 2 no. 2, pp. 164-168.

Lloyd, D. G.; Besier, T. F. (2003): An emg-driven musculoskeletal model to estimate muscle forces and knee joint moments *in vivo*. *Journal of Biomechanics*, vol. 36, no. 6, pp. 765-776.

Marquardt, D. (1963): Analgorithm for least-squares estimation of nonlinear parameters. *SIAM Journal on Applied Mathematics*, vol. 11, pp. 431-441.

Masarati, P.; Morandini, M.; Fumagalli, A. (2014): Control constraint of underactuated aerospace systems. *Journal of Computational and Nonlinear Dynamics*, vol. 9, no. 2, pp. 021014-021014.

Maugh, L. C. (1946): *Statically Indeterminate Structures*. J. Wiley & Sons. New York, USA.

Mussa-Ivaldi, F. A.; Hogan, N. (1991): Integrable solutions of kinematic redundancy via impedance control. *International Journal of Robotics Research*, vol. 10, no. 5, pp. 481-491.

Pfeifer, S.; Hardegger, M.; Vallery, H.; List, R.; Foresti, M. et al. (2011): Model-based estimation of active knee stiffness. *IEEE International Conference on Rehabilitation Robotics*, vol. 2011, pp. 5975474.

Pfeifer, S.; Vallery, H.; Hardegger, M.; Riener, R.; Perreault, E. J. (2012): Model-based estimation of knee stiffness. *IEEE Transactions on Bio-Medical Engineering*, vol. 59, no. 9, pp. 2604-2612.

Piovesan, D.; Kolesnikov, M.; Lynch, K.; Mussa-Ivaldi, F. A. (2019): The concurrent control of motion and contact force in the presence of predictable disturbances. *Journal of Mechanisms and Robotics*, vol. 11, no. 6.

Piovesan, D.; Morasso, P.; Giannoni, P.; Casadio, M. (2013): Arm stiffness during assisted movement after stroke: the influence of visual feedback and training. *IEEE Transactions on Neural Systems and Rehabilitation Engineering*, vol. 21, no. 3, pp. 454-465.

Piovesan, D.; Pierobon, A.; Dizio, P.; Lackner, J. R. (2011): Comparative analysis of methods for estimating arm segment parameters and joint torques from inverse dynamics. *Journal of Biomechanical Engineering*, vol. 133, no. 3, pp. 031003.

Piovesan, D.; Pierobon, A.; DiZio, P.; Lackner, J. R. (2012): Measuring multi-joint stiffness during single movements: numerical validation of a novel time-frequency approach. *PLoS One*, vol. 7, no. 3, pp. e33086.

Piovesan, D.; Pierobon, A.; DiZio, P.; Lackner, J. R. (2013): Experimental measure of arm stiffness during single reaching movements with a time-frequency analysis. *Journal of Neurophysiology*, vol. 110, no. 10, pp. 2484-2496.

Piovesan, D.; Pierobon, A.; Mussa Ivaldi, F. A. (2013): Critical damping conditions for third order muscle models: implications for force control. *Journal of Biomechanical Engineering*, vol. 135, no. 10, pp. 101010.

Rack, P. M.; Westbury, D. R. (1969): The effects of length and stimulus rate on tension in the isometric cat soleus muscle. *Journal of Physiology*, vol. 204, no. 2, pp. 443-460.

Salisbury, K. (1987): Whole-arm manipulation. *Proceedings of the 4th International Symposyum on Robotics Research*.

Scott, S. H.; Brown, I. E.; Loeb, G. E. (1996): Mechanics of feline soleus: I. Effect of fascicle length and velocity on force output. *Journal of Muscle Research and Cell Motility*, vol. 17, no. 2, pp. 207-219.

Segalman, D. J. (2007): Model reduction of systems with localized nonlinearities. *Journal of Computational and Nonlinear Dynamics*, vol. 2, no. 3, pp. 249-266.

Shai, O. (2011): The correction to grubler criterion for calculating the degrees of freedoms of mechanisms. *ASME 2011 International Design Engineering Technical Conferences and Computers and Information in Engineering Conference*, pp. 413-416.

Shao, Q.; Bassett, D. N.; Manal, K.; Buchanan, T. S. (2009): An emg-driven model to estimate muscle forces and joint moments in stroke patients. *Computers in Biology And Medicine*, vol. 39, no. 12, pp. 1083-1088.

Shin, H.; Lee, S.; In, W.; Jeong, J. I.; Kim, J. (2010): Kinematic optimization of a redundantly actuated parallel mechanism for maximizing stiffness and workspace using taguchi method. *Journal of Computational and Nonlinear Dynamics*, vol. 6, no. 1, pp. 011017-011017.

Spivak, M. (2018): *Calculus on Manifolds: A Modern Approach to Classical Theorems of Advanced Calculus*. CRC press. USA.

Stadlmayr, D.; Witteveen, W.; Steiner, W. (2015): Reduction of physical and constraint degrees-of-freedom of redundant formulated multibody systems. *Journal of Computational and Nonlinear Dynamics*, vol. 11, no. 3, pp. 031010-031010.

Van Bolhuis, B.; Gielen, C. (1999): A comparison of models explaining muscle activation patterns for isometric contractions. *Biological Cybernetics*, vol. 81, no. 3, pp. 249-261.

Wojtyra, M.; Frączek, J. (2012): Comparison of selected methods of handling redundant constraints in multibody systems simulations. *Journal of Computational and Nonlinear Dynamics*, vol. 8, no. 2, pp. 021007-021007.

Yamaguchi, G.; Sawa, A.; Moran, D.; Fessler, M.; Winters, J. (1990): A survey of human musculotendon actuator parameters. *Multiple Muscle Systems: Biomechanics and Movement Organization*, pp. 717-773.

Supplementary material

Table A: Implemented muscles location in our model

1	anconeus
2	short head of bicheps brachii
3	long head of bicheps brachii
4	brachialis
5	brachio-radialis
6	coraco-brachialis
7	acromial deltoid
8	clavicular deltoid
9	spinal deltoid
10	extensor carpii radialis brevis
11	extensor carpii radialis longus
12	flexor carpii radialis
13	flexor carpii ulnaris
14	serratus anterior
15	lumbar latissimus dorsii
16	sacral latissimus dorsii
17	thorax latissimus dorsii
18	teres major
19	infraspinatus
20	levetor scapulae
21	palmaris longus
22	abdominal pectoralis major
23	clavicular pectoralis major
24	sternal pectoralis major

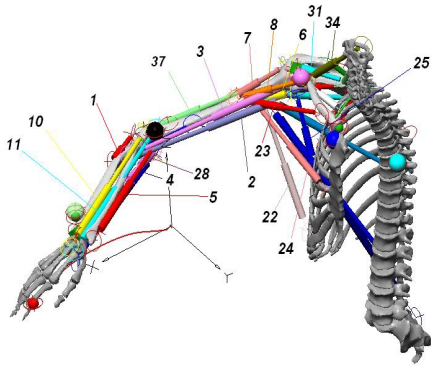

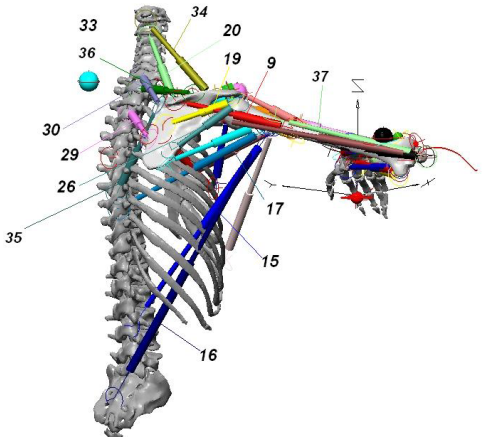

25	pectoralis minor
26	teres minor
27	pronator quadratus
28	pronator teres
29	rhomboid major
30	rhomboid minor
31	supraspinatus
32	subscapularis
33	subclavius
34	upper trapezius
35	lower trapezius
36	middle trapezius
37	lateral head of triceps brachii
38	long head of triceps brachii
39	medial head of triceps brachii

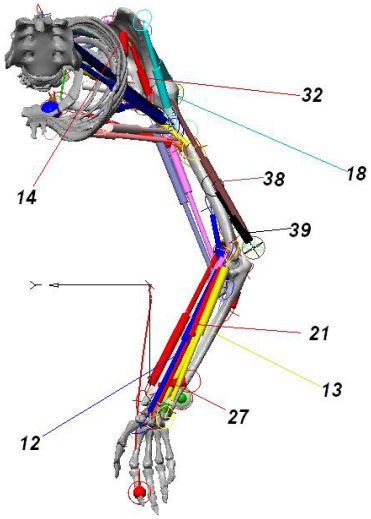

Table B: Configurations of the arm pose during the movement

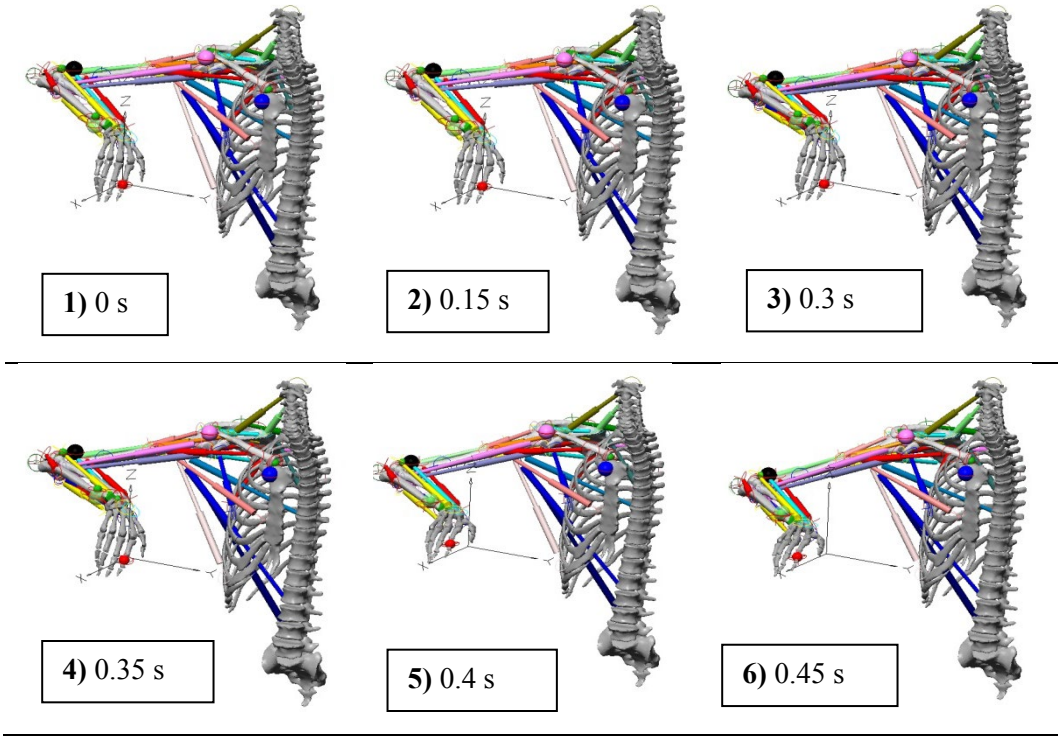

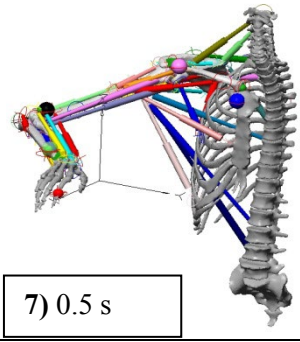

7) 0.5 s

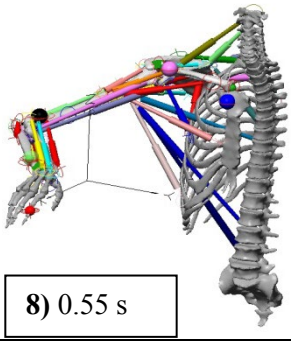

8) 0.55 s

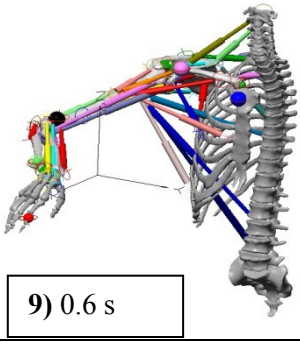

9) 0.6 s

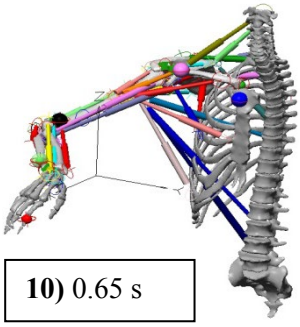

10) 0.65 s

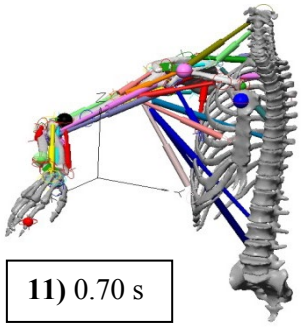

11) 0.70 s

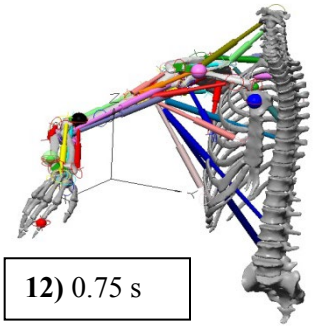

12) 0.75 s

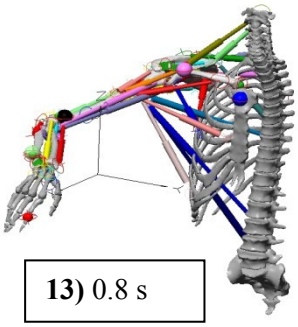

13) 0.8 s

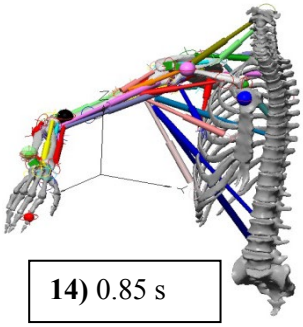

14) 0.85 s

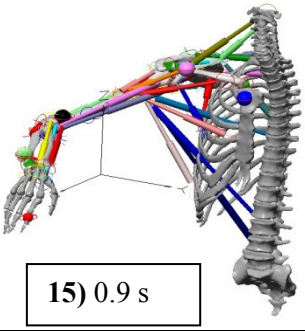

15) 0.9 s

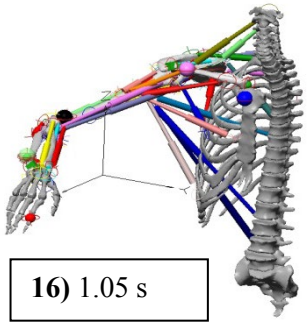

16) 1.05 s

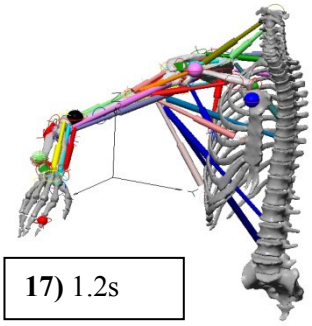

17) 1.2s

Table C: Physiological parameters of muscles [Yamaguchi, Sawa, Moran et al. (1990)].

Muscles' name	Mass [g]	x_0^T [cm]	x_0 [cm]	PCSA [cm^2]	ϕ_0 [N]	x_{path} [cm]	x_{max} [x_0]	U_r	% s.f.	% f.f.
anconeus	7.1	6.7	2.7	2.50	78.91	9.5	1.14	0.8	30.0	70.0
shor head of bicheps brachii	32.0	19.0	13.0	73.80	73.85	34.3	1.24	0.8	50.0	50.0
long head of bicheps brachii	60.0	18.0	13.6	4.20	132.35	33.9	1.23	0.8	42.3	57.7
brachialis	62.9	4.0	8.0	7.40	235.72	13.4	1.19	0.8	50.0	50.0
brachio-radialis	44.0	13.0	16.0	2.60	82.50	30.8	1.15	0.8	39.8	60.2
coraco-brachialis	22.6	8.0	10.0	2.10	67.74	18.5	1.09	0.8	50.0	50.0
acromial deltoid	236.2	3.0	16.5	430.80	430.81	20.0	1.04	0.8	53.3	46.7
clavicular deltoid	93.8	3.0	10.0	281.40	281.40	15.0	1.21	0.8	61.0	39.0
spinal deltoid	80.0	3.0	19.5	123.00	123.08	24.0	1.08	0.8	50.0	50.0
extensor carpii radialis brevis	16.7	25.0	5.3	3.00	94.80	30.0	1.15	0.8	50.0	50.0
extensor carpii radialis longus	19.4	22.5	7.8	2.30	74.61	31.0	1.21	0.8	50.0	50.0
flexor carpii radialis	12.4	22.4	5.8	64.10	64.14	28.0	1.13	0.8	50.0	50.0
flexor carpii ulnaris	16.4	23.0	4.8	102.50	102.50	28.0	1.25	0.8	50.0	50.0
serratus anterior	163.6	3.0	17.3	284.20	284.17	23.0	1.17	0.8	50.0	50.0
lumbar latissimus dorsii	120.0	5.0	31.3	115.00	115.02	41.6	1.18	0.8	50.0	50.0
sacral latissimus dorsii	120.0	12.0	34.0	105.90	105.88	51.9	1.19	0.8	50.0	50.0
thorax latissimus dorsii	120.0	2.0	28.0	128.60	128.57	33.0	1.11	0.8	50.0	50.0
teres major	75.4	4.0	12.2	185.50	185.54	18.0	1.16	0.8	44.6	55.4
infraspinatus	91.2	4.0	15.0	182.50	182.48	21.0	1.15	0.8	50.0	50.0
levator scapulae	18.8	4.0	7.0	80.60	80.64	12.0	1.17	0.8	50.0	50.0
palmaris longus	5.5	21.0	5.7	28.90	28.95	27.0	1.21	0.8	50.0	50.0
abdominal pectoralis major	83.4	4.0	20.3	123.10	123.07	28.5	1.21	0.8	50.0	50.0
clavicular pectoralis major	100.0	2.0	18.0	5.20	166.77	22.0	1.12	0.8	42.3	57.7
sternal pectoralis major	102.5	3.0	21.3	144.30	144.34	28.0	1.18	0.8	43.1	56.9
pectoralis minor	55.6	6.0	13.5	123.60	123.56	21.0	1.13	0.8	50.0	50.0
teres minor	26.3	3.0	10.4	75.80	75.79	15.0	1.17	0.8	50.0	50.0
pronator quadratus	14.0	1.5	4.0	105.00	105.00	6.0	1.14	0.8	50.0	50.0
pronator teres	29.8	6.0	7.0	127.71	127.71	14.0	1.18	0.8	50.0	50.0
romboid major	43.8	4.0	11.4	115.07	115.07	17.0	1.15	0.8	50.0	50.0
romboid minor	29.8	4.0	7.9	113.63	113.63	13.0	1.17	0.8	50.0	50.0
supraspinatus	42.0	2.5	8.6	146.11	146.11	12.0	1.11	0.8	50.0	50.0
subscapularis	129.7	4.0	12.2	319.32	319.32	18.0	1.16	0.8	50.0	50.0
subclavius	18.0	2.0	7.6	70.87	70.87	11.5	1.26	0.8	50.0	50.0
upper trapezius	85.1	6.0	12.5	204.29	204.29	19.0	1.06	0.8	50.0	50.0
lower trapezius	211.9	3.0	20.7	307.87	307.87	24.0	1.02	0.8	50.0	50.0
middle trapezius	95.5	8.0	12.7	225.69	225.69	21.0	1.05	0.8	50.0	50.0
lateral head of triceps brachii	50.1	18.0	8.4	179.04	179.04	27.1	1.18	0.8	32.5	67.5
long head of triceps brachii	70.6	24.5	10.2	207.65	207.65	36.3	1.26	0.8	65.5	34.5
medial head of triceps brachii	41.0	9.5	6.3	195.33	195.33	17.0	1.26	0.8	32.5	67.5

Tab. C represent the physiological parameters of muscles used in the simulation of VM. The main variables are described as follows Mass (g): Mass of the muscle fascia in grams.

- x_0(cm): Average length of the fascicles in the muscle fascia, when the muscle is at its optimal length for production of isometric tetanic force. -PCSA cm^2: Physiological cross-sectional area of the muscle. - ϕ_0 N: The maximal amount of force that the muscle can produce isometrically. -x_0^T cm: Length of the tendon at the muscle's optimal force. x_{path} cm: Maximum length of the whole- muscle (i.e., entire musculotendon path length) at the most extreme anatomical position. -$x_{max}(x_0)$: The maximal length of the fascicles at extreme anatomical position of the skeleton, measured in terms of the optimal fascicle length. -U_r: Fractional excitation level at which all motor units for a given muscle are recruited. -Number_unit: The number of motor units assigned to each slow twitch and fast twitch fiber type. -%s.f.: percentage of slow twitching fibers -%f.f.: Percentage of fast twitching fibers.